

Computational study of the stable atomic trapping sites in Ar lattice

Georgiy K. Ozerov¹, Dmitry S. Bezrukov^{1,2}, and Alexei A. Buchachenko¹

¹*Skolkovo Institute of Science and Technology, Skolkovo Innovation Center, Building 3, Moscow 143026, Russia*

E-mail: g.ozarov@skoltech.ru

a.buchachenko@skoltech.ru

²*Department of Chemistry, M.V. Lomonosov Moscow State University, Moscow 119991, Russia*

Received October 24, 2018

Stable atomic trapping sites in the Lennard-Jones face-centered cubic Ar crystals are investigated by means of the global optimization strategy and convex hull concept for thermodynamic stability. Five generic site types are found in full accord with crystallographic intuition: interstitial within tetrahedral and octahedral hollows and substitutions, single, tetra- and hexavacancy. Their identities are established by radial distribution function analysis. Stability regions of these sites are mapped into the space of Lennard-Jones parameters of the guest–host interatomic interaction. Predictions made for the number and types of the stable sites for selected atoms (H, Mn, Na, Yb, Eu, Ba) are found to be in line with the results of more sophisticated models and matrix isolation spectroscopy experiments.

Keywords: rare gas solids, trapping site, guest–host interaction.

1. Introduction

Studies of atomic species isolated in rare gas (RG) solids are of interest in many fundamental and applied respects. For atomic physics, they complement characterization of the interatomic interactions and electronic energy transfer pathways [1], can give atomic structure parameters unavailable from gas-phase experiments [2], and occasionally provide highly sensitive detection schemes [3]. For solid state physics and chemistry, they serve as the models of the structure, mobility and electronic properties of the point defects, as well as of the reactivity in solids [4–6].

Most of these links rely on the fact that in the free standing RG crystals or carefully prepared RG matrices guest atoms occupy well-defined, sometimes multiple, stable trapping sites. Evidences are numerous, see, for instance, Refs. 7–17. However, the structure and energy of such sites can hardly be established from experiment alone. Among rare exceptions are the ESR experiments in Xe matrices depleted or enriched in nuclear spin-bearing isotopes, which allowed Feldman and co-workers prove the existence of interstitial and substitutional sites for hydrogen atoms [7]. Partial resolution of the phonon structure of the narrow b^4D , a^4D and a^6D emission bands of atomic manganese by McCaffrey group [8,9] revealed the tetrahedral (T_d) and octahedral (O_h) symmetry of the host envi-

ronment for two sites observed. Energy order of three stable sites occupied by Yb in Ar were established from the light- and heat-induced site interconversion kinetics [10]. Of course, classical modeling is very helpful for trapping site characterization, especially if addresses kinetic [11,18] or thermodynamic [10,19] stability of the predicted sites.

Fortunately, crystallographic intuition helps a lot. It tells [1] that the face-centered cubic (fcc) RG lattice offers guest atom G two hollows for interstitial (IS) occupation, T_d and O_h (ISTd and ISOH hereinafter), single substitution (SS), as well as two larger vacancies with substitution of four (vertex plus three face-centered) or six (all face-centered) lattice atoms, tetra- and hexavacancies (TV and HV), respectively. Knowing effective volumes of the respective voids in the ideal lattice, one can easily judge which one fits the effective volume of atom G (given, e.g., by the G–RG equilibrium distance) better. There are strong indications that other occupations are at least much less probable. They never appear in the models as the low energy or stable sites. All the “intuitive” accommodations possess high symmetry that unavoidably leads to characteristic triplet Jahn–Teller structure of the $S \rightarrow P$ absorption and excitation bands. It becomes a custom to explain the lack of such structure in the spectra and assign the bands with different shapes to atoms located at grain boundaries and other defects [12]. However, the powerful intuitive arguments do

not account for lattice relaxation, which may well contribute to minimization of the accommodation energy and eventually lead to counter-intuitive structures.

Does a handful of “intuitive” accommodations really exhaust all the variety of stable sites to be found in solid rare gases? Is the volume matching criterion reliable enough for judging their stability? Could one expect other typical sites and what would be their spectral signatures? The importance of the answers goes beyond atomic matrix isolation being related to a wider context of the defect and impurity distributions in crystalline materials. Of course, the answers cannot be given at the mathematical rigor. Instead, one can seek them in a “maximum likelihood” sense under certain restrictions. Rapidly developing field of computational structure prediction, see, e.g., Refs. 20–22, provides useful recipes.

In the present contribution we report on the computational search of the thermodynamically stable atomic trapping sites in the Ar crystal. As an atomistic model, we used the one proposed before [10,19]. It describes an ideal crystal, but provides enough flexibility for accommodating a guest in the vacancies of different volume. In line with the previous experience in modeling RG clusters and solids, e.g., Refs. 23–30, we used simple Lennard-Jones (LJ) interaction potentials. Aside of known inaccuracies arising from non-negligible many-body interactions in RG crystals [31,32], this assumption excludes from consideration guest atoms bearing non-zero electron orbital angular momentum for their anisotropic interaction with host atoms. Furthermore, we work with potential energy instead of free energy. Entropy and work contributions can be accounted for, but for the present qualitative analysis they may not be decisive, while require atomic mass to be introduced as an extra variable dimension.

After setting up the model with the fixed interaction within the host crystal, we embed guest atom G into various vacancies of the fixed discrete “volume”, measured in the number of host atoms $N \geq 0$ dislodged from the lattice. The G–Ar LJ interaction parameters vary in a reasonably wide range. Performing global optimization, we define the site structures with the lowest energy. Using the convex hull concept [33] adapted to present case of N as the phase variable, we identify the stability of the structures found. The result is the map of stable sites of the volume N in the two-dimensional space of LJ parameters. Additional step is the structure analysis across the parameter space, which allows us to identify distinct site structures of the same volume.

This approach gives the solid proof that “intuitive” accommodations are indeed most probable candidates to the stable atomic trapping sites. Our stability maps allow one to guess the site stability knowing just the equilibrium distance and binding energy of the guest–host interaction potential. The certainty of such predictions is confirmed for several atoms investigated with more accurate potential models and experimentally.

2. Computational methods

2.1. Model

The model for trapping site structure and stability used here is an extension of the approach introduced in Refs. 10 and 19. Its starting point is the (large) set of Ar atoms that forms the fragment of an ideal fcc crystal, as optimized with the particular pairwise Ar–Ar interaction potential. The set is confined by an outer surface close to the sphere and is further subdivided in two sets. The first one, bound by another concentric surface of the smaller size, contains movable atoms, whose positions may vary, manually at the sampling or naturally under the action of classical forces from other atoms during optimization. The fixed atoms belong to the second set and are located between two surfaces. They always keep their lattice positions. Thus, Ar atoms of the movable set can adapt themselves to the force induced by embedded atom G, while the atoms of fixed set maintain the long-range periodic order of the host crystal. In contrast to our previous applications [10,19], where the sizes of the sets were chosen once by convergency of the results, we need here more flexibility to handle the variation of the guest–host interaction potential automatically. So the present model allows for slight tuning at each potential parameter choice, as described in the Sec. 2.2 below.

Trapping of the host atom G is assumed to occur in the central region, where it can substitute few host atoms. The number of Ar atoms dislodged from the system by embedded guest, $N \geq 0$, serves as the parameter of the model and as the discrete descriptor of the trapping volume. Potential energy of so prepared system, $U_{G@Ar}(N; \mathbf{x})$, is subjected to global optimization with respect to coordinates of all movable atoms \mathbf{x} to find (more precisely, approximate) global minimum $E_{G@Ar}(N)$, which represents the most favorable trapping site for a given volume N . The corresponding accommodation energy is equal to

$$\Delta E(N) = E_{G@Ar}(N) - E_{Ar} + NE^{at}, \quad (1)$$

where the second term is the energy of original ideal Ar crystal and the third term is the energy cost of removal of Ar atoms proportional to the crystal atomization energy per atom. Eq. (1) ties all accommodation energies to the common energy zero, ideal crystal plus free atom.

The minimum of ΔE as function of N , $\Delta E(N_0)$, corresponds to the ground trapping site. Other thermodynamically stable sites can also be found if one identifies potential energy with the free energy of defect formation, omitting the work against pressure for removal of Ar atoms and entropy contribution. Here we follow this approximation avoiding additional parameter (the mass of atom G) and aiming a qualitative overview. Thus, $\Delta E(N)$ is directly related to the convex hull analysis of the discrete composition phase diagrams in crystal structure investigation [33].

In our particular case, the structure with some $N \neq N_0$, whose energy ΔE belongs to the convex hull of the $(N, \Delta E(N))$ graph, is considered as thermodynamically stable (or N -stable). Considered are $N \leq 15$.

To describe Ar–Ar interaction, we used LJ potential as the function of interatomic distance r :

$$u_{\text{Ar}}(r) = \varepsilon_{\text{Ar}} \left[\left(\frac{\rho_{\text{Ar}}}{r} \right)^{12} - 2 \left(\frac{\rho_{\text{Ar}}}{r} \right)^6 \right], \quad (2)$$

with the parameters adjusted to the gas-phase semiempirical potential by Aziz [34], namely, equilibrium distance $\rho_{\text{Ar}} = 3.76 \text{ \AA}$ and binding energy $\varepsilon_{\text{Ar}} = 100 \text{ cm}^{-1}$. This potential approximates relevant crystal parameters as $a = 5.17 \text{ \AA}$ and $E^{\text{at}} = 861 \text{ cm}^{-1}$, worse than the original potential function [34] ($a = 5.20 \text{ \AA}$, $E^{\text{at}} = 787 \text{ cm}^{-1}$). One can also recall the values from the “best pairwise” *ab initio* calculations [32], $a = 5.21 \text{ \AA}$ and $E^{\text{at}} = 760 \text{ cm}^{-1}$, which, being amended by three- and four-body contributions and vibrational zero-point energy correction, accurately reproduces experimental data [35,36] $a = 5.311 \text{ \AA}$ and $E^{\text{at}} = 646 \text{ cm}^{-1}$.

The potential for G–Ar interaction, u_{G} , has the same LJ form with the scalable ρ and ε parameters. We vary the former from 1.9 to 5.5 \AA with the linear step of 0.08 \AA , and the latter from 10 to 1000 cm^{-1} as the geometric progression with the common ratio 1.01 and scale factor 20.

2.2. Sampling and optimization

Global optimization problem for a certain potential energy surface requires extensive sampling of the configuration space. Present application to the family of the potential energy surfaces adds the requirements of uniform convergence in the energy calculation and in the sampling efficiency. To satisfy these criteria, we use the following way to set up crystal model sketchly introduced above.

Within the starting ideal crystal we first define the central set containing all atoms whose distance from the center does not exceeding $2a$. The whole atomic set included in the modelling is then determined by energetic criterion. Namely, it includes all atoms whose minimum pairwise interaction with the atoms in the central set exceeds the maximum interaction of two atoms within the central set by eight orders of magnitude. The most distant atoms satisfying this condition and forming the convex three-dimensional envelope are designated as the surface atoms. They form outer boundary of the crystal fragment and define its average radius R . Numerous tests confirmed that it is safe to keep Ar atoms located $5R/6$ or longer from the center as fixed. All the rest atoms, including those of the central set, are considered as movable.

The first presampling stage takes an advantage of the periodic nature of the problem. Within the central region, we define the auxiliary “vacancy” lattice, which includes all lattice nodes, as well as natural tetrahedral and octahe-

dral hollows, and is geometrically equivalent to the spatial body-centered cubic lattice with the constant $a/4$. Then all possible placements of the guest atom G in the vacancy lattice, accompanied by removal of N host atoms and replacements of the others within empty nodes, are probed and their energies are computed for the particular choice of G–Ar interaction parameters ρ and ε . The configuration with the lowest energy is identified (in case of geometrically equivalent degenerated configurations, the one in which G atom is closest to the center is chosen). For this particular configuration, the pairwise energy condition for the surface atoms is checked taking into account G–Ar contributions. If not satisfied, the whole atomic set is enlarged and the sets of movable and fixed host atoms are redefined accordingly. This makes the model dependent on the G–Ar potential and N . However, as the energy of the ideal crystal E_{Ar} in Eq. (1) is always calculated for the same model as $E_{\text{G@Ar}}(N)$, the resulting relative accommodation energy values $\Delta E(N)$ are all given at the same scale.

The second global optimization stage relies on the simulated annealing (SA) method based on Metropolis algorithm [37–39] seeded by the preselected structure. Few hundred of cooling steps are made, each consist of few hundred random walks involving all atoms in the central region followed by the steepest descent geometry refinement [39]. The lowest energy configuration found in this process is considered as an approximation to the ground minimum for the central set.

At third stage, resulting configuration is refined by the steepest descent minimization of the positions of all movable atoms, including those outside the central set. The latter are slightly displaced randomly to avoid trapping in the highly symmetric initial positions.

Repeating the procedures of the model setup, sampling, global and local optimizations, we collect the atomic configurations with the lowest energy in the space $(N; \rho, \varepsilon)$ for further analysis.

2.3. Structure analysis

The set of accommodation energies $\Delta E(N)$ (1) obtained for each G–Ar potential is analyzed using the convex hull concept and the ground structure with the minimum energy $\Delta E(N_0)$ at certain N_0 , as well as extra stable structures with distinct N (if any), are identified. As far as N is the parameter of the model, the stability of accommodations with certain N is defined uniquely in the space of the potential parameters. More difficult is to distinguish and classify different structural types of the stable accommodations.

Here, the radial distribution functions (RDFs) are used as the main structural descriptor. We implemented smoothed RDFs in the form

$$\rho'(r) = \frac{1}{s\sqrt{\pi}} \sum_i \exp \left[-(r - |\mathbf{x}_G - \mathbf{x}_i|)^2 / s^2 \right], \quad (3)$$

where \mathbf{x}_G and \mathbf{x}_i are the position vectors of the guest atom and host atoms, the summation over i runs over all Ar atoms and the Gaussian smoothing parameter s is set to $0.1a$ for better presentation purpose. To avoid rapid accumulation of ρ' at large distances, the weight factor is applied, $\rho(r) = w(r)\rho'(r)$, $w(r) = 1/(4\pi a^2)$ if $r \leq a$ and $w(r) = 1/(4\pi r^2)$ if $r > a$.

3. Results

The map of N_0 , the volume of the ground sites, presented in the Fig. 1 has strikingly simple structure. First, it shows that the ground trapping sites can only correspond to $N_0 = 0, 1, 4$ and 6 . Our search also identified sporadic appearance of the $N = 7$ structures as the ground, but in paving parameter space it has negligible measure. Second, the volume occupied by an atom in the ground site strongly depend on interaction potential range ρ . Dependence on interaction strength is less pronounced, but becomes stronger with growing N_0 , obviously due to larger lattice relaxation effects for polyatomic vacancies.

In the Fig. 2, we map the stability regions of the sites with all N that manifests themselves as the ground sites. In addition to the (blue, dark) regions, where each $N = N_0$ and thus gives the ground sites, the regions where N gives the sites with higher energy, but still stable within the convex hull concept, are also shown (orange, light). As $N = 0$ is the endpoint of convex hull, the corresponding accommodation energy can only be compared with that of $N = 1$ sites. So the sites with $N = 0$ can be either ground or unstable (their sporadic appearance at large ρ simply means that they lie lower in energy than the $N = 1$ sites, which, in turn, are not the ground sites). All other border cases are

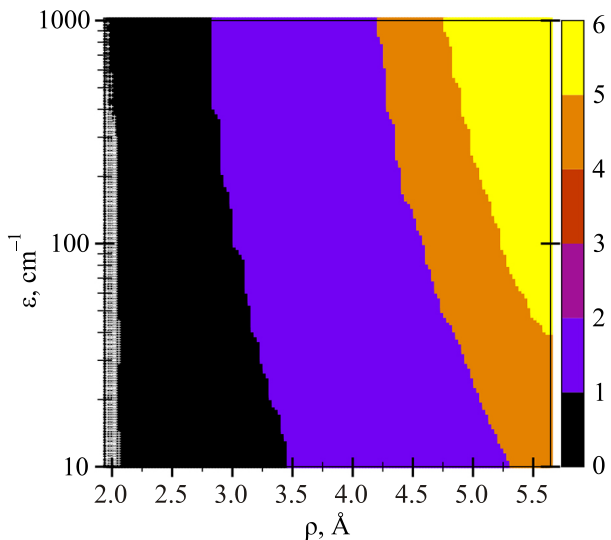


Fig. 1. (Color online) Map of the volume N_0 of the ground trapping sites in the LJ parameter space (ρ , ϵ). Right vertical bar specifies the color — N_0 correspondence. Narrow shaded region at $\rho < 2$ Å corresponds to $N_0 = 0$ tetrahedral accommodation, as established by RDF analysis (see text). Black region features $N_0 = 0$ octahedral accommodation.

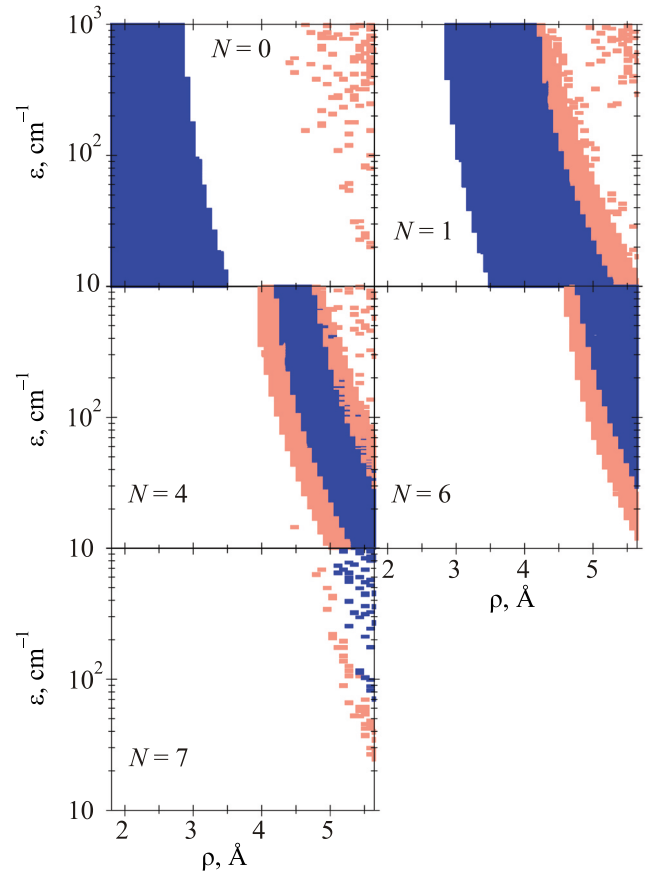


Fig. 2. (Color online) Maps of the stability regions for the trapping sites with different volume N . Orange (light) color corresponds to the thermodynamic stability regions, blue (dark) — to the regions where the sites appear as the ground.

smoother: as ρ increases, the larger site first emerges as stable above the ground one, then goes down in energy to acquire the lowest energy. Further increase of G–Ar interaction range first makes it more energetic than the newly emerging larger site and finally destabilizes it. For strong long-range G–Ar interactions (upper-right corner of the map), the small sites with $N = 0, 1$ and ones with $N = 4$ appear sporadically together with $N = 2, 3$ and 5 sites (not shown). Such sites never manifest themselves as the ground and normally have very high accommodation energies with respect to the ground site. Moreover, scattered pattern indicates that small variation of LJ potential destabilizes them, so any deviation from LJ interaction model towards more realistic potential should do the same. The sites with $N = 7$ can be considered as exception, as they may compete with smaller $N = 4$ and $N = 6$ sites for the lowest accommodation energy.

Mapping of site volume N thus reveals that only the sites with $N = 0, 1, 4$ and 6 should be considered as thermodynamically stable. Among others, theoretical possibility exists to meet occasionally $N = 7$ accommodation.

The sites of the same volume may well correspond to distinct structural types. Definition of the type is somewhat elusive requiring proper descriptors. Here we rely on the

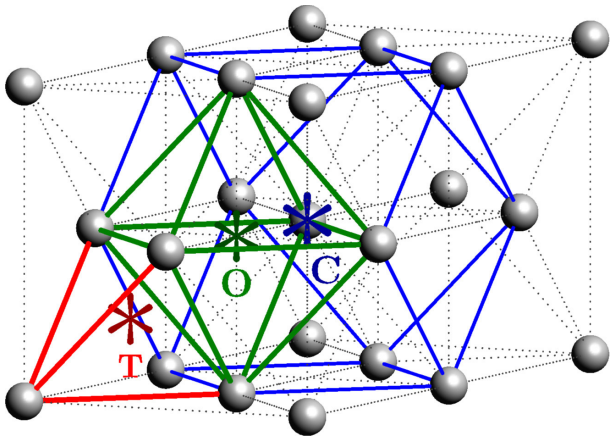


Fig. 3. (Color online) Origins of the reference RDFs for fcc lattice: tetrahedral hollow (T, red), octahedral hollow (O, green) and lattice node with cubooctahedral coordination (C, blue).

analysis of radial distribution functions (3) for the symmetry of the host environment of the trapped atom. To do so, we introduced reference RDFs $\rho_0(r)$ describing pure ideal fcc lattice. The origin \mathbf{x}_G is replaced by three crystallographic positions schematically shown in the Fig. 3, namely $(a/4, a/4, a/4)$, $(a/2, a/2, a/2)$ and $(a/2, a, a/2)$. The origins correspond, respectively, to the tetra-

dral and octahedral hollows and the lattice atom, or to “intuitive” ISTd, ISOh and SS accommodations of the guest atom. They actually exhaust the types of high-symmetry environments, tetrahedral, octahedral and cubooctahedral. Polyatomic vacancies TV and HV belong to the same types and their RDFs are the same except the disappearance of the first peak due to removal of four or six nearest lattice atoms.

In the Fig. 4 we compare the RDFs computed for all ground sites across the LJ parameter space, but differentiated in N . Looking at the relatively long-range behavior ($r > 3a/2$), one sees perfect correspondence between computed and reference distribution functions. In case of $N = 0$, two very distinct patterns exist, one closely follows the reference for tetrahedral hollow, another — for octahedral one. They obviously correspond to the interstitial ISTd and ISOh accommodations of the guest atom.

The sites with $N = 1$ reveal, asymptotically, the cubooctahedral environment. At short range $r < a$, however, the distributions are strongly blurred. Inspection shows that the site structure always corresponds to the single substitution, but the first coordination sphere inflates as the size of the guest atom ρ increases. Noteworthy, SS site can remain ground even if the closest host atoms are shifted to the distances pertinent to more spacious tetravacancy.

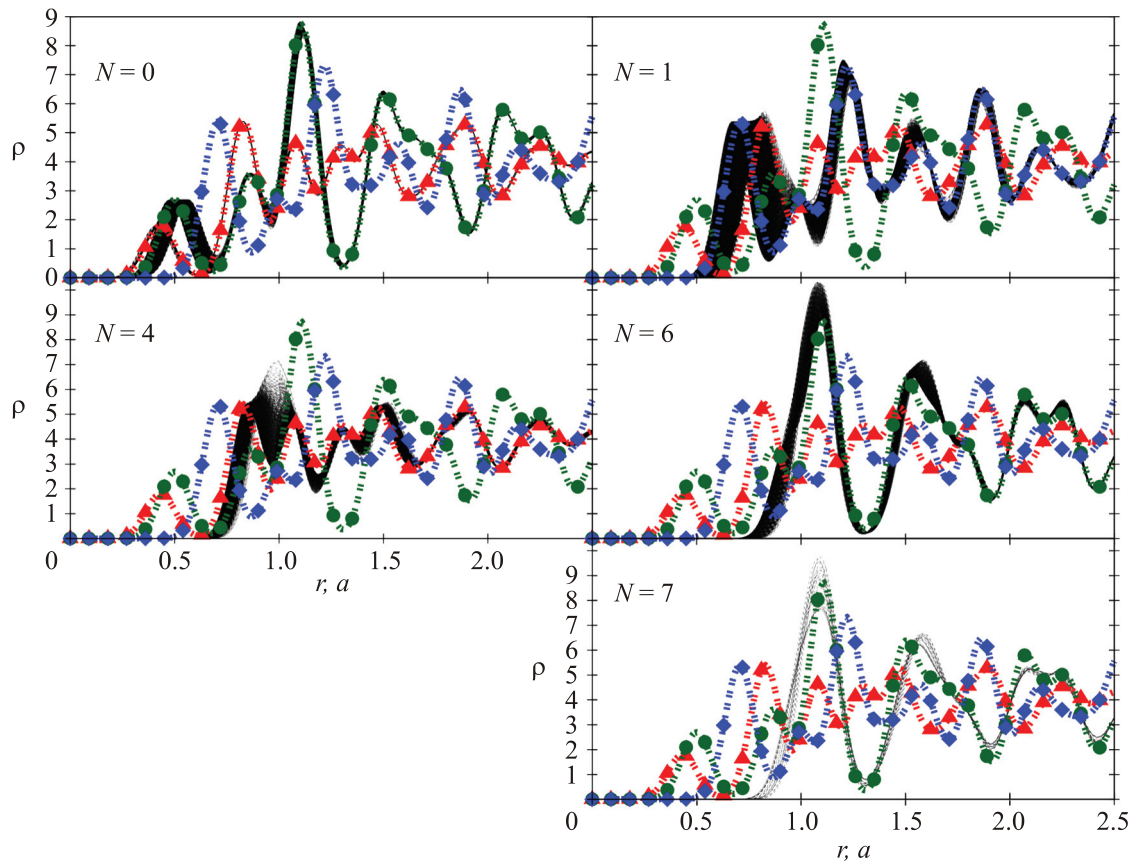


Fig. 4. (Color online) Radial distribution functions for the ground sites with certain N . Lines with symbols show the reference RDFs: red triangles for tetrahedral, green circles for octahedral and blue diamonds for cubooctahedral origins. Note that distances are given in lattice constant units a .

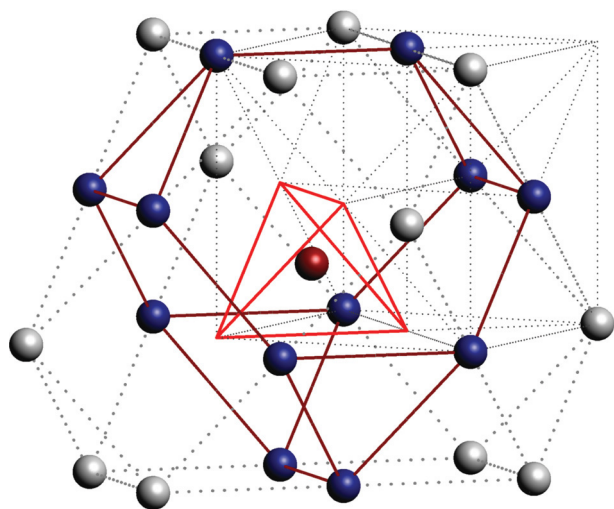


Fig. 5. (Color online) Schematic structure of the tetravacancy $N = 4$ site. Guest atom is shown as the red sphere surrounded by tetrahedron formed by removed host atoms. Blue color emphasizes 12 host atoms of the first shell, grey color — 12 atoms of the second shell.

At $N = 4$, RDFs clearly reflect the tetrahedral symmetry. The absence of the peak at short r typical to the tetrahedral reference RDF indicates TV guest atom accommodation, in which four closest lattice atoms are removed, see Fig. 5. Significant spread of the computed RDFs around $r < a$ does not reflect distinct structural types. For relatively small ρ , the first two tetrahedral shells, each consisting of 12 host atoms, remain resolved, while at larger ρ they shrink to effectively a single shell. The second-shell atoms enter to each of the four hexagonal spaces of the first shell by three compensating in part the inflation of the first shell, see Fig. 5.

The $N = 6$ case clearly corresponds to octahedral reference with the first peak absent, that is, hexavacancy. The

major peak is shifted towards shorter distances reflecting the fact that $N = 6$ stability region mainly corresponds to G–Ar interactions stronger than Ar–Ar one, see Fig. 2. Interestingly, $N = 7$ sites give very similar pattern also indicating octahedral environment. Figure 6 illustrates schematic structure of these two sites, that differ by one atom lying in the hexagonal plane of the first coordination shell. In fact, in the $N = 7$ structure guest atom is slightly displaced from the center of octahedral hollow towards the seventh atom missed. This lowers the local symmetry of its surrounding is C_{3v} .

Extension of the RDF analysis to stable sites above the ground does not bring any new insight. It is also confirmed by the structure analysis based on the complete-linkage clustering technique [40,41] for different structural metrics [42]. In addition to what is revealed by the N_0 -map, it splits one $N = 0$ stability region in two, for tetra- and octahedral interstitial accommodations, respectively. The former is roughly represented by narrow vertical band with $\rho \leq 2$ Å, as also shown in Fig. 1 for completeness. To assess the reliability of the present computational predictions, we made several comparisons for the atomic systems studied within the same thermodynamic stability model but with more sophisticated pairwise Ar–Ar and G–Ar interaction potentials. The Fig. 7 shows accommodation energies $\Delta E(N)$ (1) for Mn@Ar and Yb@Ar systems. The former was studied in Ref. 19 with the *ab initio* Mn–Ar potential function giving $\rho = 4.52$ Å and $\varepsilon = 76$ cm⁻¹. Using these parameters for LJ potential, we recomputed accommodation energies with the present model. Figure 7 confirms the correct prediction for the stable sites at $N = 1$ and 4. This is also in full agreement with experiment, which proved the existence of two sites with octahedral/cubooctahedral and tetrahedral host environment [13] established from the phonon broadening [8,9]. Another example studied in similar way [10] is Yb@Ar with *ab initio* values $\rho = 5.03$ Å and

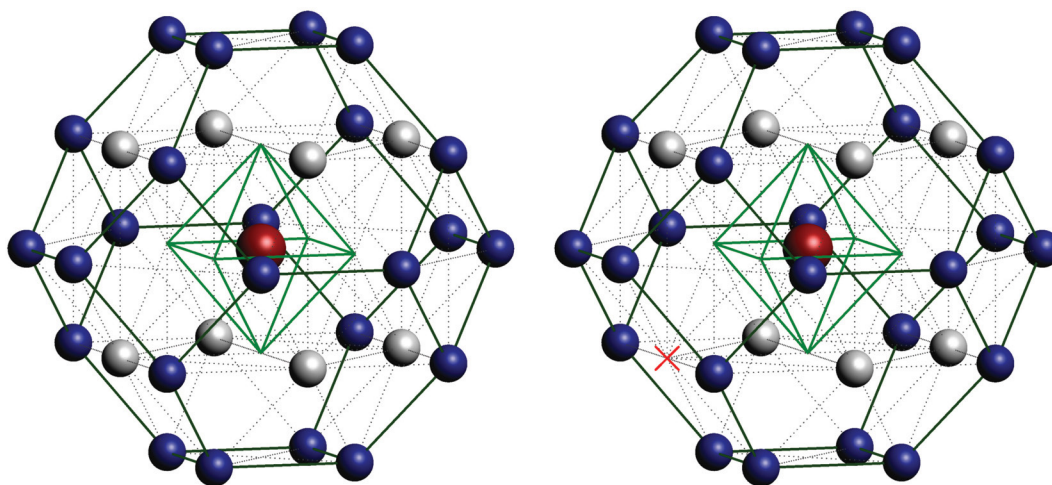


Fig. 6. (Color online) Schematic structures of the hexavacancy $N = 6$ site (left) and $N = 7$ site (right). Guest atom is shown as the red sphere surrounded by octahedron formed by six removed host atoms. Blue and grey colors emphasize host atoms belonging to first and second shells, respectively. On the right panel, position of the seventh atom missed for $N = 7$ is marked by the cross.

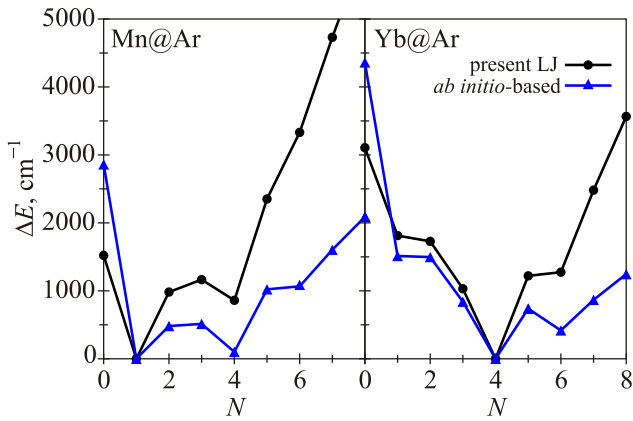


Fig. 7. (Color online) Accommodation energies for Mn@Ar (left) and Yb@Ar (right) computed with the *ab initio*-based and LJ potential models.

$\varepsilon = 69 \text{ cm}^{-1}$. Figure 7 again indicates good qualitative agreement for stable sites. Existence of three stable sites and their energy ordering $\text{TV} \leq \text{HV} \ll \text{SS}$ predicted by the *ab initio*-based model [10] are confirmed experimentally [10]. Quantitative difference between the present LJ and *ab initio* models is remarkable. It roots not only in the quality of G–Ar interaction potentials, but also in the deficiency of Ar–Ar LJ potential, which produces host lattice tighter than the original potential function [34] does.

Qualitative account of the stable sites found for these and some other atoms studied with *ab initio*-based G–Ar interactions and Ar–Ar interactions by Aziz [34], namely, H, Na, Eu and Ba, is summarized in Table 1. Note that information from the present model is deduced simply by picking particular (ρ, ε) point on the stability maps in Fig. 2.

To some extent, excellent agreement between theoretical models can find indirect support from experimental data. Hydrogen atom in RG matrices is known to occupy two types of traps [7,15–17]. One releases the atoms at moderate heating, while the atoms in the second remain trapped. Assuming that they correspond to the IS and SS accommodations, respectively, and taking into account that hydrogen mobility in Ar is suppressed, we can regard our

result as consistent with observations. The Na@Ar system had been a subject of numerous studies, which agree in existence of three stable trapping sites. Combined experimental-theoretical study [11] tentatively assigned the ground “blue” site to TV (this site was also found to be most stable kinetically), second “violet” site — to SS, and “red” one — to HV. Our stability analysis performed with the same Na–Ar potential fully supports this assignment, whereas the LJ stability maps are not certain about $N = 6$ HV site, which falls just on the border of stability region at our resolution. In view of this, alternative assignment of the “red” site to grain boundary occupation [43] looks less plausible. “Red” and “blue” sites were observed and ascribed to HV and TV accommodations of Eu in Ar [14]. The dominant one was assumed to be HV, as more spacious hexavacancy in the ideal lattice better fits large Eu atom. According to our simulations, lattice deformation reverses the trend and makes initially less favorable tetrahedral vacancy more beneficial than HV. Excitation-emission spectroscopy of Ba in Ar revealed four sites, with three of them giving characteristic triplet Jahn–Teller structure of excitation bands [14]. Preliminary results of the site stability analysis with the *ab initio* Ba–Ar potentials from Ref. 44 indicates favorable HV and TV accommodations and high-lying SS structure as the candidates. Present maps reproduce HV and TV, but put SS on the border of stability region. Thus, aside of few subtleties, present maps provide quite reliable guidelines for site assignments.

4. Conclusions

Structure and stability of the atomic trapping sites in the fcc Ar crystal are addressed by means of global optimization strategy. Pairwise Lennard-Jones interaction potential energy surface and convex hull thermodynamic stability criterion are employed. Stable trapping sites are characterized by the effective discrete “volume” (the number of host atoms dislodged) and radial distribution functions that reflects the symmetry of the host environment. Detailed maps in the space of guest–host LJ interaction parameters are produced for stability of all types of the sites found.

Table 1. Qualitative comparison of the stable trapping sites for selected atoms in Ar investigated using the *ab initio*-based models and predicted from the present stability maps

Atom	$\rho, \text{Å}$	$\varepsilon, \text{cm}^{-1}$	Present map	<i>Ab initio</i> -based
H	3.59	33	$N_0 = 1, \text{SS}$	$N_0 = 1, \text{SS}$
Mn	4.52	76	$N_0 = 1, \text{SS}; N = 4, \text{TV}$	$N_0 = 1, \text{SS}; N = 4, \text{TV}^a$
Na	4.99	42	$N_0 = 1, \text{SS}; N = 4, \text{TV}$	$N_0 = 1, \text{SS}; N = 4, \text{TV}; N = 6, \text{HV}$
Yb	5.03	69	$N_0 = 4, \text{TV}; N = 6, \text{HV}; N = 1, \text{SS}$	$N_0 = 4, \text{TV}; N = 6, \text{HV}; N = 1, \text{SS}^b$
Eu	5.22	66	$N_0 = 4, \text{TV}; N = 6, \text{HV}$	$N_0 = 4, \text{TV}; N = 6, \text{HV}; N = 1, \text{SS}^c$
Ba	5.58	64	$N_0 = 6, \text{HV}; N = 4, \text{TV}$	$N_0 = 6, \text{HV}; N = 4, \text{TV}; N = 1, \text{SS}^c$

Notes: ^a Ref. 19; ^b Ref. 10; ^c High-energy site.

Our approach fully confirms the “intuitive” crystallographic assumptions. Only five generic types of stable sites are found:

- (i), (ii) interstitial within tetrahedral and octahedral hollows (ISTd and ISO_h);
- (iii) single substitution (SS);
- (iv) tetravacancy substitution accompanied by removal of vertex and three nearest face-centered host atoms (TV);
- (v) hexavacancy substitution accompanied by removal of six face-centered host atoms (HV).

Other trapping sites appear on the map sporadically and unlikely can be regarded as observable. Interesting exception is the $N = 7$ substitutional site emerging, also sporadically, as the ground accommodation. It is the only candidate to the ground structure that has axial symmetry, lower than T_d or O_h .

The maps allow one to establish the most probable accommodation knowing just equilibrium parameters of the guest–host interaction. As illustrated by comparison with more sophisticated theoretical models and experimental findings, such prediction is more precise than that based on effective volumes of vacancies and hollows in ideal lattice. Indeed, radial distribution functions show that first shell may undergo significant deformation to adapt itself to embedded guest atom.

Finally, one should stress on the scalability of the LJ model. It can be formulated in the space of reduced parameters, ρ/ρ_{Ar} and $\varepsilon/\varepsilon_{Ar}$ and applied to any fcc crystal that can be adequately described by the pairwise LJ potential. It makes the generic trapping site types confirmed above “universal”, at least for rough preliminary interpretation. We do not explore this aspect here as it requires more careful selection of the parameter grids, finer tuning of atomic crystal model and perhaps more sophisticated approaches to structural type characterization.

We thank Sean McCaffrey for providing unpublished data and interest to the work and Daniil Izmodenov for preliminary study of H@Ar. This work was supported by Russian Science Foundation (project no. 17-13-01466).

1. C. Crépin-Gilbert and A. Tramer, *Int. Rev. Phys. Chem.* **18**, 485 (1999).
2. C.-Y. Xu, J. Singh, J.C. Zappala, K.G. Bailey, M.R. Dietrich, J.P. Greene, W. Jiang, N.D. Lemke, Z.-T. Lu, P. Mueller, and T.P. O’Connor, *Phys. Rev. Lett.* **113**, 033003 (2014).
3. B. Mong, S. Cook, T. Walton, C. Chambers, A. Craycraft, C. Benitez-Medina, K. Hall, W. Fairbank, Jr., J.B. Albert, D.J. Auty, P.S. Barbeau, V. Basque, D. Beck, M. Breidenbach, T. Brunner, G.F. Cao, B. Cleveland, M. Coon, T. Daniels, S.J. Daugherty, R. DeVoe, T. Didberidze, J. Dilling, M.J. Dolinski, M. Dunford, L. Fabris, J. Farine, W. Feldmeier, P. Fierlinger, D. Fudenberg, G. Giroux, R. Gornea, K. Graham, G. Gratta, M. Heffner, M. Hughes, X.S. Jiang, T.N. Johnson, S. Johnston, A. Karelin, L.J. Kaufman, R. Killick, T. Koffas, S. Kravitz, R. Krücken, A. Kucherkov, K.S. Kumar, D.S.

- Leonard, C. Licciardi, Y.H. Lin, J. Ling, R. MacLellan, M.G. Marino, D. Moore, A. Odian, I. Ostrovskiy, A. Piepke, A. Pocar, F. Retiere, P.C. Rowson, M.P. Roza, A. Schubert, D. Sinclair, E. Smith, V. Stekhanov, M. Tarka, T. Tolba, K. Twelker, J.-L. Vuilleumier, J. Walton, M. Weber, L.J. Wen, U. Wichoski, L. Yang, Y.-R. Yen, and Y.B. Zhao (nEXO Collaboration), *Phys. Rev. A* **91**, 022505 (2015).
4. G.L. Pollack, *Rev. Mod. Phys.* **36**, 748 (1964).
5. R.N. Perutz, *Chem. Rev.* **85**, 97 (1985).
6. V.A. Apkarian and N. Schwentner, *Chem. Rev.* **99**, 1481 (1999).
7. V.I. Feldman, F.F. Sukhov, and A.Y. Orlov, *J. Chem. Phys.* **128**, 214511 (2008).
8. O. Byrne, M.A. Collier, M.C. Ryan, and J.G. McCaffrey, *Fiz. Nizk. Temp.* **36**, 524 (2010) [*Low Temp. Phys.* **36**, 417 (2010)].
9. M.A. Collier, O. Byrne, C. Murray, and J.G. McCaffrey, *J. Chem. Phys.* **132**, 164512 (2010).
10. L.-G. Tao, N.N. Kleshchina, R. Lambo, A.A. Buchachenko, X.-G. Zhou, D.S. Bezrukov, and S.-M. Hu, *J. Chem. Phys.* **143**, 174306 (2015).
11. M. Ryan, M. Collier, P. de Pujo, C. Crépin, and J.G. McCaffrey, *J. Phys. Chem. A* **114**, 3011 (2010).
12. B.M. Davis, B. Gervais, and J.G. McCaffrey, *J. Chem. Phys.* **148**, 124308 (2018).
13. M.A. Collier and J.G. McCaffrey, *J. Chem. Phys.* **122**, 054503 (2005).
14. O. Byrne and J.G. McCaffrey, *J. Chem. Phys.* **134**, 124501 (2011).
15. T. Miyazaki, A. Wakahara, T. Usui, and K. Fueki, *J. Phys. Chem.* **86**, 3881 (1982).
16. M. Beyer, E.V. Savchenko, G. Niedner-Schatteburg, and V.E. Bondybey, *Fiz. Nizk. Temp.* **25**, 1087 (1999) [*Low Temp. Phys.* **25**, 814 (1999)].
17. K. Vaskonen, J. Eloranta, T. Kiljunen, and H. Kunttu, *J. Chem. Phys.* **110**, 2122 (1999).
18. C. Crépin, P. de Pujo, B. Bouvier, V. Brenner, and P. Millié, *Chem. Phys.* **272**, 243 (2001).
19. N.N. Kleshchina, K.A. Korchagina, D.S. Bezrukov, and A.A. Buchachenko, *J. Phys. Chem. A* **121**, 2429 (2017).
20. J.C. Schön and M. Jansen, *Angew. Chem. Int. Ed. Engl.* **35**, 1288 (1996).
21. S.M. Woodley and R. Catlow, *Nature Mater.* **7**, 937 (2008).
22. *Modern Methods of Crystal Structure Prediction*, A.R. Oganov (ed.), Berlin, Wiley-VCH (2010).
23. A.J. Stone, *The Theory of Intermolecular Forces*, Clarendon, Oxford (1996).
24. J.S. Brown, *Proc. Phys. Soc. (London)* **89**, 987 (1966).
25. F.W. de Wette and R.M.J. Cotterill, *Solid State Commun.* **6**, 227 (1968).
26. C. Malinowska-Adamska, P. Sloma, and J. Tomaszewski, *Phys. Status Solid. B* **200**, 451 (1997).
27. L.T. Wille, *Ann. Rev. Comput. Phys.* **VII**, 25 (2000).
28. B. Hartke, *Angew. Chem. Int. Ed.* **41**, 1468 (2002).
29. H. Putz, J.C. Schön, and M. Jansen, *Ber. Buns. Ges. Phys. Chem.* **99**, 1148 (1995).

30. J.C. Schön, H. Putz, and M. Jansen, *J. Phys.: Condens. Matter* **8**, 143 (1996).
31. P. Schwerdtfeger, B. Assadollahzadeh, and A. Hermann, *Phys. Rev. B* **82**, 205111 (2010).
32. K. Rościszewski, B. Paulus, P. Fulde, and H. Stoll, *Phys. Rev. B* **62**, 5482 (2000).
33. Q. Zhu, A.R. Oganov, and P.B. Allen, *Phys. Rev. B* **87**, 195317 (2013).
34. R.A. Aziz, *J. Chem. Phys.* **99**, 4518 (1993).
35. L.A. Schwalbe, R.K. Crawford, H.H. Chen, and R.A. Aziz, *J. Chem. Phys.* **66**, 4493 (1977).
36. O.G. Peterson, D.N. Batchelder, and R.O. Simmons, *Phys. Rev.* **150**, 703 (1966).
37. N. Metropolis, A.W. Rosenbluth, M.N. Rosenbluth, A.H. Teller, and E. Teller, *J. Chem. Phys.* **21**, 1087 (1953).
38. P.J.M. van Laarhoven and E.H.L. Aarts, *Simulated Annealing: Theory and Applications*, Springer, Dordrecht (1987).
39. *Search Methodologies: Introductory Tutorials in Optimization and Decision Support Techniques*, E.K. Burke and G. Kendall (eds.), 2nd ed., Springer, Boston MA (2014).
40. F.H. Allen, M.J. Doyle, and R. Taylor, *Acta Cryst. B* **47**, 41 (1991).
41. P. Dawyndt, H.D. Meyer, and B.D. Baets, *Soft Computing* **9**, 385 (2003).
42. G.K. Ozerov, D.S. Bezrukov, and A.A. Buchachenko, *to be published*.
43. E. Jacquet, D. Zanuttini, J. Douady, E. Giglio, and B. Gervais, *J. Chem. Phys.* **135**, 174503 (2011).
44. A.A. Buchachenko and L.A. Viehland, *J. Chem. Phys.* **148**, 154304 (2018).

Обчислювальні дослідження стійких пасток атомів в ґратці аргону

Г.К. Озеров, Д.С. Безруков, О.А. Бучаченко

Для дослідження стабільних пасток атомів в гранецентрованої кубичній ґратці аргону, що моделюється потенціалами Леннарда-Джонса, використано методи глобальної оптимізації та оцінки термодинамічної стійкості за методом опуклих оболонок. У повній відповідності з інтуїтивними кристало-

графічними міркуваннями виявлено пастки п'яти загальних типів: залучення в тетраедричні та октаедричні порожнини ґратки, заміщення її вузла та заміщення чотирьох- та шести-атомних вакансій. Індивідуальність цих типів встановлена за результатом аналізу радіальних функцій розподілу атомів ґратки. Представлено карти областей стійкості пасток всіх типів в просторі параметрів взаємодії Леннарда-Джонса між захопленим атомом та атомом ґратки. Передбачення числа й типів стійких пасток атомів H, Mn, Na, Yb, Eu та Ba, які отримано на основі карт, узгоджуються з результатами більш точних моделей та доступних експериментів з матричної ізоляції.

Ключові слова: тверді інертні гази, пастка, взаємодія гість–господар.

Вычислительное исследование устойчивых ловушек атомов в решетке аргона

Г.К. Озеров, Д.С. Безруков, А.А. Бучаченко

Для исследования стабильных ловушек атомов в гранецентрированной кубической решетке аргона, моделируемой потенциалами Леннарда-Джонса, использованы методы глобальной оптимизации и оценки термодинамической устойчивости по методу выпуклых оболочек. В полном соответствии с интуитивными кристаллографическими соображениями обнаружены ловушки пяти общих типов: внедрения в тетраэдрическую и октаэдрическую полости решетки, замещение ее узла и замещения четырех- и шестиатомных вакансий. Индивидуальность этих типов установлена в результате анализа радиальных функций распределения атомов решетки. Представлены карты областей устойчивости ловушек всех типов в пространстве параметров взаимодействия Леннарда-Джонса между захваченным атомом и атомом решетки. Предсказания числа и типов устойчивых ловушек атомов H, Mn, Na, Yb, Eu и Ba, полученные на основе карт, согласуются с результатами более точных моделей и доступных экспериментов по матричной изоляции.

Ключевые слова: твердые инертные газы, ловушка, взаимодействие гость–хозяин.